AD-A174 932 ALGEBRAIC GRID GENERATION FOR AN AFTERBODY WITH FINITE 1/1
SPAN TAPERED FINS(U) PENNSYLVANIA STATE UNIV STATE
COLLEGE APPLIED RESEARCH LAB G H HOFFMAN OCT 86
UNCLASSIFIED ARL/PSU/TR-86-007 F/G 1/3 NL

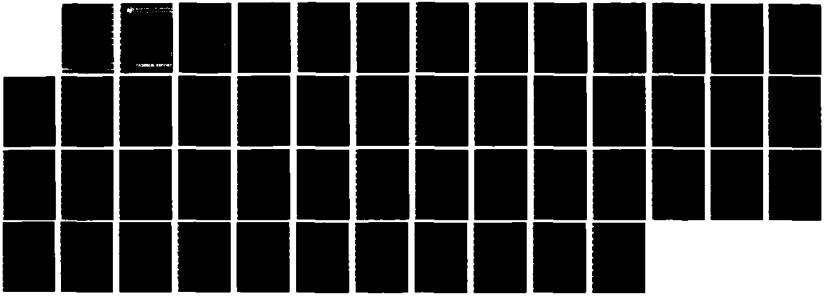

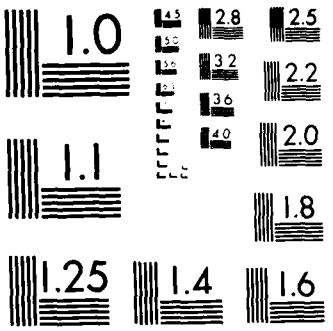

Applied Research Laboratory
The Pennsylvania State University

(10)

ALGEBRAIC GRID GENERATION FOR AN AFTERBODY WITH FINITE SPAN, TAPERED FINS

by

G. H. Hoffman

ARLPSU

TECHNICAL REPORT

10

The Pennsylvania State University
Intercollege Research Programs and Facilities
APPLIED RESEARCH LABORATORY
P. O. Box 30
State College, PA 16804

ALGEBRAIC GRID GENERATION FOR AN AFTERBODY WITH FINITE SPAN, TAPERED FINS

by

G. H. Hoffman

Technical Report TR 86-007
October 1986

Supported by: Naval Sea Systems Command

L. R. Hettche, Director
Applied Research Laboratory

Unclassified
SECURITY CLASSIFICATION OF THIS PAGE

AD-A174 932

REPORT DOCUMENTATION PAGE

1a. REPORT SECURITY CLASSIFICATION Unclassified	1b. RESTRICTIVE MARKINGS
2a. SECURITY CLASSIFICATION AUTHORITY	3. DISTRIBUTION/AVAILABILITY OF REPORT
2b. DECLASSIFICATION/DOWNGRADING SCHEDULE	
4. PERFORMING ORGANIZATION REPORT NUMBER(S)	5. MONITORING ORGANIZATION REPORT NUMBER(S)
6a. NAME OF PERFORMING ORGANIZATION Applied Research Laboratory The Penna. State University	6b. OFFICE SYMBOL (If applicable) ARL
7a. NAME OF MONITORING ORGANIZATION Naval Sea Systems Command Department of the Navy	
6c. ADDRESS (City, State, and ZIP Code) P. O. Box 30 State College, PA 16804	7b. ADDRESS (City, State, and ZIP Code) Washington, DC 20362
8a. NAME OF FUNDING/SPONSORING ORGANIZATION Naval Sea Systems Command	8b. OFFICE SYMBOL (If applicable) NAVSEA
9. PROCUREMENT INSTRUMENT IDENTIFICATION NUMBER	
8c. ADDRESS (City, State, and ZIP Code) Department of the Navy Washington, DC 20362	10. SOURCE OF FUNDING NUMBERS

PROGRAM ELEMENT NO.	PROJECT NO.	TASK NO.	WORK UNIT ACCESSION NO.

11. TITLE (Include Security Classification)

Algebraic Grid Generation for an Afterbody with Finite Span, Tapered Fins

12. PERSONAL AUTHOR(S)
G. H. Hoffman

13a. TYPE OF REPORT	13b. TIME COVERED	14. DATE OF REPORT (Year, Month, Day)	15. PAGE COUNT
Technical	FROM _____ TO _____	October 1986	49

16. SUPPLEMENTARY NOTATION

17. COSATI CODES			18. SUBJECT TERMS (Continue on reverse if necessary and identify by block number)
FIELD	GROUP	SUB-GROUP	3-D grid generation, pointed afterbody, fins

19. ABSTRACT (Continue on reverse if necessary and identify by block number)

An algebraic technique is presented for the generation of a 3-D grid about a pointed afterbody with four tapered, finite span fins. The grid topology is largely determined by a polar type singularity which passes through the tip parallel to the body centerline. A 3-D grid is generated by stacking a sequence of 2-D grids on predetermined "blank" surfaces in the fin and tip regions. On each blank surface a grid of the C-type is computed by a combination of conformal mapping and transfinite interpolation. The method is an extension of previous work for the generation of a 3-D grid about an afterbody with four constant chord, infinite span fins. An example grid is presented to illustrate the method and its characteristics are discussed.

20. DISTRIBUTION/AVAILABILITY OF ABSTRACT	21. ABSTRACT SECURITY CLASSIFICATION
☒ UNCLASSIFIED/UNLIMITED ☐ SAME AS RPT. ☐ DTIC USERS	Unclassified
22a. NAME OF RESPONSIBLE INDIVIDUAL	22b. TELEPHONE (Include Area Code) / 22c. OFFICE SYMBOL

DD FORM 1473, 84 MAR

83 APR edition may be used until exhausted.
All other editions are obsolete.

SECURITY CLASSIFICATION OF THIS PAGE
Unclassified

Abstract: An algebraic technique is presented for the generation of a 3-D grid about a pointed afterbody with four tapered, finite span fins. The grid topology is largely determined by a polar type singularity which passes through the tip parallel to the body centerline. A 3-D grid is generated by stacking a sequence of 2-D grids on predetermined "blank" surfaces in the fin and tip regions. On each blank surface a grid of the C-type is computed by a combination of conformal mapping and transfinite interpolation. The method is an extension of previous work for the generation of a 3-D grid about an afterbody with four constant chord, infinite span fins. An example grid is presented to illustrate the method and its characteristics are discussed.

Acknowledgment: This work was sponsored jointly by ONR Code 432, NSEA 63R-31, and NSEA 55W33 under the auspices of the Accelerated Research Option on Hull Propulsor Interaction.

TABLE OF CONTENTS

NOMENCLATURE

c	airfoil chord length
c_R	root chord - see Fig. 3
c_T	tip chord - see Fig. 3
d_{BOD}	length of afterbody
d_{IVL}	distance from fin leading edge to initial value surface - see Fig. 4
d_{IVLO}	distance from fin leading edge to initial value surface on centerline - see Fig. 3
d_{OB}	distance from tail to outflow surface
d_S	distance inside airfoil from leading edge to singularity of unwrapping transformation
d_{TL}	distance from trailing edge of fin to tail of afterbody - see Fig. 3
r_B	afterbody radius
r_{B1}	initial afterbody radius
r_M	radius of tubular grid surface
r_{OC}	outer cylinder radius - see Fig. 3
r_T	tip radius - see Fig. 3
x,r,θ	cylindrical coordinates
x,y,z	Cartesian coordinates
x_R	distance from root leading edge to generator line origin - see Fig. 4
u,v	hinge plane coordinates - see Eq. (12)
y_M	ordinate of fin-tubular surface intersection - see Fig. 5
z_F	fin airfoil thickness - see Fig. 5
ξ,η	normalized coordinates used in transfinite interpolation

Δy	parameter in one-dimensional stretching function
$\hat{\eta}$	running arc length of radial curve
ϕ_o	turning angle at point O - see Fig. 9
$\hat{\theta}_T$	half angle at tail of afterbody
τ	airfoil thickness, fraction of chord length
ζ	normalized polar variable in azimuthal plane - see Eq. (26)

All other quantities are defined in the text.

LIST OF FIGURES

LIST OF TABLES

1. INTRODUCTION

Algebraic methods have become firmly established over the past decade as an effective means of producing grids about complex three-dimensional (3-D) geometries. Truly 3-D approaches of this type all involve some form of interpolation to determine a grid on the interior of a given domain which may or may not be divided into simpler sub-domains. Eriksson [1] has generated a single-block nonorthogonal 3-D grid using transfinite interpolation where geometric data are specified only on the boundaries. Since no internal surfaces are specified, grid quality is controlled, especially near a surface, by incorporating out-of-surface derivatives. Smith et. al. [2] simplify the 3-D grid generation process by using the building block concept where several adjoining or partially overlapping physical grids map to a computational cube. On the interior of each building block transfinite interpolation is used to generate the grid. Their treatment extends only to the wing tips which limits its usefulness. Multi-surface interpolation methods have been highly developed by Eiseman [3]. In this technique intermediate control surfaces (not coordinate surfaces) are introduced between bounding surfaces in order to provide a high degree of control over mesh properties near boundaries.

The second category of algebraic techniques involves stacking methods, i.e., the generation of a 3-D grid by a sequence of 2-D operations. In this procedure a set of surfaces is determined by some form of mapping and then a grid is generated on each surface in such a way as to maintain smoothness across surfaces. This approach works well when the geometry is simple in one of the three spatial dimensions. The

efforts of Caughey and co-workers [4,5] are representative in this area. They develop a boundary-conforming coordinate system by a sequence of conformal and shearing transformations to yield a nearly orthogonal computational domain. The grid is then generated by simple linear interpolation. This technique has seen considerable application in transonic flow calculations over fighter aircraft configurations. Conformal mapping in conjunction with stacking has also been exploited by Halsey [6] to generate grids about 3-D nacelles with and without other aircraft components in close proximity.

One of the advantages of the stacking approach over its 3-D interpolation counterpart is that appropriate conformal mapping can be used to eliminate corners at boundaries. Such a technique was used by Hoffman [7] for a 3-D stacked grid about an afterbody of circular cross-section with four constant chord fins. Hoffman's method consists of applying a hinge point transformation to the entire boundary in the unwrapping process for a given grid surface.

In this report the method of Ref. 7 is extended to the case of tapered, finite span fins. The type of afterbody is the same as in Ref. 7, namely, one of circular cross-section that closes at the tail point. Gridless surfaces are first determined free of corner singularities and then a grid is generated on each surface by a sequence of conformal transformations in conjunction with transfinite interpolation. The topology of this configuration being more complex than that of Ref. 7 requires the domain to be divided into two regions - above and below the tip of the fin. The nature of the grid in the region between the body and tip dictates the introduction of a singularity of

the polar type at the tip. This singularity forms the basis of the coordinate system for the grid outside the tip. Such singularities are a necessary occurrence in 3-D grids although they are not restricted to the polar type. For a discussion of this feature of 3-D grids, see Ref. 1.

2. ANALYSIS

2.1 Geometry of Computational Domain

The geometry for which a surface fitted grid is to be generated is as follows:

(1) The afterbody is of circular cross-section and has a smooth but otherwise arbitrary meridian profile that closes at the tail point.

(2) Four identical finite span fins are mounted on the afterbody at 90 degree intervals with their chord planes passing through the afterbody centerline. The leading and trailing edges are straight with only the leading edge having taper. The tip is formed by revolving the airfoil at the end of the fin about the tip axis.

(3) The computational domain consists of the region interior to an outer cylinder of radius r_{OC} and exterior to the afterbody, bounded upstream and downstream by planes normal to the afterbody centerline (the initial value and outflow planes).

A schematic of the body-fin geometry and computational domain is shown in Fig. 1, a head-on view showing the coordinate system in the azimuthal plane appears in Fig. 2 and a meridian plane view of the configuration showing parameters defining the geometry appears in Fig. 3.

Since the fins are identical and equally spaced, there are four planes of symmetry and hence, only the azimuthal sector - $\pi/4 \leq \theta \leq 0$ needs to be considered in generating the grid and in the flowfield computation.

2.2 Overall Approach

The grid generation process is divided into two parts. The first is for the fin (or inner) region which lies within the tip cylinder, while the second is for the tip (or outer) region which lies between the tip cylinder and the outer cylinder. The method used in the inner region is a direct extension of that in Ref. 7 for a constant chord fin. "Blank" axisymmetric surfaces (with no grid) are first created which vary smoothly in the radial direction from the afterbody to the tip cylinder. On each of these surfaces a C-grid about the fin is then determined by 2-D means with controls to maintain grid smoothness in the radial direction. In the outer region a coordinate system with a polar singularity is used to gain maximum grid resolution in the vicinity of the tip. This type of singularity is also dictated by the nature of the grid in the fin region. The polar axis is taken to pass through the tip centerline and is therefore a generator of the tip cylinder. Blank grid surfaces (curved radial surfaces) are created which emanate from the polar singularity and which have the property of being invariant with respect to translation along the polar axis. A C-grid around the tip is then determined by 2-D means on each curved radial surface. The grids in the outer and inner regions are of course required to be the same at their common surface, the tip cylinder.

2.3 Fin Region

Tubular Surfaces

The first step in the grid generation process is the determination of a set of blank (gridless) surfaces, also called "tubular" surfaces, between the body and tip cylinder. These surfaces are generated by computing a set of curves in the meridian plane using the method of Ref. 7 and then revolving them about the centerline. Once the intersection of a given surface with the fin is known, the surface is "unwrapped" in terms of x and θ coordinates by ignoring the radial variation with x of the surface. A C-grid is then computed in the x-θ plane by using the conformal mapping-transfinite interpolation procedure described in Ref. 7.

Because of fin taper the computation of the fin-tubular surface intersection is more complicated than in the constant chord case of Ref. 7. For the tapered case the determination of the intersection (which yields the distorted airfoil coordinates in the x-θ plane for use in determining the C-grid) proceeds as follows:

As shown in Fig. 4, the fin is defined to originate on the body centerline and because of its truncated triangular shape has a "virtual" tip at T', the point where extensions of the leading and trailing edges intersect. To generate the curve of intersection of the fin with a given tubular surface, all points defining the intersection are assumed to lie on generators which are lines passing through T' and intersecting the centerline at a distance x_R from the root leading edge. This artifice enables the airfoil thickness distribution to be computed only once and then used for all chord locations because every chord plane distribution

is geometrically similar. Taking the origin at the leading edge of the fin root, the equation of a generator line is

$$\hat{x} = x_R + \left(\frac{c_R - x_R}{y_{T'}}\right) \hat{y} , \tag{1}$$

where

$$y_{T'} = \frac{r_T}{1 - c_T / c_R} . \tag{2}$$

In applying Eq. (1), the distribution of x_R is determined from the unit chord airfoil distribution x_{Fl} by the relation

$$x_R = c_R \, x_{Fl} . \tag{3}$$

The equation of the tubular surface in the meridian plane may be written as

$$r = r_M(x) . \tag{4}$$

Replacing y in Eq. (1) by r_{Mi} the difference $(\hat{x} - x_i)$ is computed for points on the meridian curve. Then using Lagrange cubic interpolation, the zero (root) of $(\hat{x} - x_i)$ is found from which $\hat{x}$ of the intersection and r_{Mi} are computed. We note that $\hat{x}$ must be used in the root finding process rather than $\hat{y}$ because the $\hat{y}$ equation becomes indeterminate at the leading edge.

To determine the appropriate chord length (which enables the airfoil thickness at the point of intersection to be found) we refer to Fig. 5 which is a sketch of the fin-tubular surface intersection in the azimuthal plane. Because of the geometric similarity property of all chord point distributions, we have

$$z_F = c\, z_{F1} \quad , \tag{5}$$

where z_F is the airfoil thickness at the intersection point and z_{F1} is the airfoil thickness for the unit chord distribution. The airfoil chord, c, is given by

$$c_R = c_R - a\, y_M \quad , \tag{6}$$

where y_M is the projection of r_M on the fin plane of symmetry, and

$$a = \frac{c_R - c_T}{r_T} \quad . \tag{7}$$

The quantities r_M, y_M and z_F are related by

$$r_M^2 = y_M^2 + z_F^2 \quad . \tag{8}$$

By using Eqs. (5) and (6) to eliminate z_F and c, we can solve Eq. (8) for y_M with the following result:

$$y_M = \frac{ac_R z_{F1}^2 + [(ac_R z_{F1})^2 + (1 + az_{F1}^2)\,(r_M^2 - c_R^2\, z_{F1}^2)]^{1/2}}{a + az_{F1}^2} \quad . \tag{9}$$

With y_M known, c and z_F are computed from Eqs. (6) and (5) respectively. The quantity d_{IVL}, the distance from the initial value line (IVL) to the fin leading edge required in the C-grid generation step, is given by

$$d_{IVL} = d_{IVLO} + a\, y_{MLE} \quad , \tag{10}$$

where d_{IVLO} is the IVL - fin leading edge distance on the centerline and y_{MLE} is given by Eq. (9) applied at the fin leading edge.

Grid on Tubular Surfaces

Since the procedure used to generate the C-grid on an unwrapped tubular surface is essentially the same as in Ref. 7, only the outline of the main steps will be presented. The portions of the original procedure which have been modified for the present application are described in detail.

Starting in the x-θ plane a sequence of conformal transformations unwraps the airfoil, symmetry lines and initial and outflow lines into a quadrilateral with slowly varying height. Next, a translation and rotation of coordinates is made about the image of the airfoil trailing edge and a hinge point transformation applied to eliminate the corner at the trailing edge. The boundary in the hinge plane is now smooth with a slowly vary tangent and is thus suitable for producing a grid in its interior by interpolation. Transfinite interpolation using cubic blending functions is used for this task producing a smooth grid orthogonal at all boundaries. The grid in the x-θ plane is then obtained by reversing the sequence of transformations. Finally, the grid on the tubular surface is found by determining by Lagrange interpolation the tubular radius corresponding to the x-coordinate of each grid point in the x-θ plane.

Spacing of grid points on the boundaries made up of the stagnation line, airfoil and wake centerline is determined in physical coordinates by using one-dimensional stretching functions, as described in Ref. 7. Grid points on the outflow line are determined in the hinge plane also in the manner of Ref. 7. Placement of grid points on the initial value line and 45 degree symmetry line is presently accomplished by requiring points

on these boundaries in the hinge plane (the north boundary) to be spaced in the same arc length proportion as points on the south boundary (the image of the stagnation line, airfoil and wake centerline). The present method is guaranteed to produce a non-folded grid whereas the older circular arc method of Ref. 7, which is also applied in the hinge plane, sometimes produces folding in the vicinity of the stagnation line in the case of thick airfoils.

The method of locating point K has also been changed. Point K (see Fig. 6) is the intersection of the grid line emanating from point C (the intersection of the inflow and 45 degree symmetry lines). In Ref. 7 the circular arc method was used to locate point K automatically whereas in the present application point K is specified in physical coordinates as part of the input. The new procedure provides more flexibility for the division of grid lines intersecting the airfoil from the initial value and 45 degree symmetry lines.

2.4 TIP REGION

Curved Radial Surfaces

The topology of the radial curves emanating from the tip polar axis is illustrated in Fig. 7. The constraints that must be satisfied are that orthogonality exists at intersections with the outer and 45 degree symmetry boundaries (segments A-E and E-D) and that the curve from O to E bisects the angle at E. These curves, upon translation in the x direction, create radial surfaces for the grid in the tip region.

The radial curves are generated by a variant of the conformal mapping-transfinite interpolation procedure used for the grid on

tubular surfaces in the fin region. With origin at point E, a hinge point transformation is applied to straighten out segment A-E-D, viz.

$$w = z^2 \quad , \tag{11}$$

where

$$z = x + iy \quad , \tag{12}$$

$$w = u + iv \quad . \tag{13}$$

This transformation guarantees that the angle at point E will be bisected by the line which intersects it. Applying the transformation to the entire bounding curve O-D-E-A-O produces a three-cornered boundary in the u-v plane, as illustrated in Fig. 8. Transfinite interpolation with cubic blending functions is then used to create lines emanating from point O which are normal to A-E-D. Because the north boundary collapses to point O with the result that $(\vec{r}_\xi)_0 = 0$ and $(\vec{r}_{\xi\eta})_0 = 0$, the transfinite interpolation relation, Eq. (26) of Ref. 7, reduces to (using point-of-compass notation and labeling corners as shown in Fig. 8)

$$\begin{aligned}
\vec{r}(\xi, \eta) = {} & \vec{r}_s(\xi)\, E(\eta) + \vec{r}_0\, F(\eta) + \vec{r}_{\eta s}(\xi) G(\eta) + \vec{r}_{\eta O}(\xi)\, H(\eta) \\
& + E(\xi)\, [\vec{r}_w(\eta) - \vec{r}_A\, E(\eta) - \vec{r}_0\, F(\eta) - \vec{r}_{\xi WA}\, G(\eta) - \vec{r}_{\xi WO}\, H(\eta)] \\
& + F(\xi)\, [\vec{r}_E(\eta) - \vec{r}_D\, E(\eta) - \vec{r}_0\, F(\eta) - \vec{r}_{\xi ED}\, G(\eta) - \vec{r}_{\xi EO}\, H(\eta)] \\
& + G(\xi)\, [\vec{r}_{\xi W}(\eta) - \vec{r}_{\xi WA}\, E(\eta) - \vec{r}_{\xi\eta WA}\, G(\eta)] \\
& + H(\xi)\, [\vec{r}_{\xi E}(\eta) - \vec{r}_{\xi ED}\, E(\eta) - \vec{r}_{\xi\eta ED}\, G(\eta)] \quad .
\end{aligned} \tag{14}$$

where E, F, G and H are cubic blending functions given by

$$\left.\begin{aligned} F(u) &= u^2(3 - 2u) \\ G(u) &= u(1 - u)^2 \\ H(u) &= u^2(u - 1) \\ E(u) &= 1 - F(u) \end{aligned}\right\} . \qquad (15)$$

The normalized variables ξ and η are defined as follows: On segment A-E-D,

$$\xi_i = sl_i/sl_{total} , \qquad (16)$$

and on segment A-O,

$$\eta_j = s2_j/s2_{total} , \qquad (17)$$

where sl_i and $s2_j$ are the running arc lengths on A-E-D and O-A respectively, as measured from point A.

The arc length on the various boundaries is computed from the chord formula using a dense point distribution to obtain as much accuracy as possible. The desired point distribution on A-E-D, which is much less dense than that used to determine arc length, is computed using uniform increments in θ on A-E and uniform increments in x on E-D (see Fig. 7).

The corresponding sl_i is then obtained by Lagrange cubic interpolation on u_i from which ξ_i is computed. The distribution of η is arbitrary as it is used only to define the radial curves for later use. The method presently is use is to specify uniform increments in u on A-O, from which corresponding values of v, x and y are determined analytically.

The evaluation of the various derivatives in the transfinite interpolation relation is analogous to that in Ref. 7 with one

exception. At point 0 the turning angle ϕ_0 of ξ = constant lines, defined in Fig. 9, is a prescribed function of ξ. Then at point 0 the unit tangent vector is given by

$$\vec{t}_1(\xi) = \cos \phi_0 \, \vec{e}_u - \sin \phi_0 \, \vec{e}_v \tag{18}$$

where $\vec{e}_u$ and $\vec{e}_v$ are unit tangent vectors in the u and v directions respectively.

If A-E-D were a segment of a circle and the radial lines from point 0 were straight, then ϕ_o and ξ would be related by

$$\phi_0(\xi) = \phi_0(0) + \frac{\pi}{2} \cdot \xi \tag{19}$$

Figure 10 shows a typical set of radial curves generated using the above relation. In the vicinity of O-E folding occurs brought on by the rapidly changing curvature of A-E-D in the hinge plane near point E which cannot be handled adequately by transfinite interpolation. This defect can be cured without changing Eq. (19) by following a strategy devised by Vinokur & Lombard [8], namely, incorporation of an interior stretching function in ξ which produces clustering at point E. We define:

$$\bar{\xi} = \bar{\xi}\,(\xi) \quad , \tag{20}$$

and then perform transfinite interpolation in $(\bar{\xi},\eta)$ variables. The derivatives affected in Eq. (14) are $\vec{r}_\xi$ and $\vec{r}_{\xi\eta}$ which now become $\vec{r}_{\bar{\xi}}$ and $\vec{r}_{\bar{\xi}\eta}$. The new derivatives are related to the old by

$$\vec{r}_{\bar{\xi}} = \vec{r}_{\xi} \; / \; \frac{d\bar{\xi}}{d\xi} \; , \tag{21}$$

and

$$\vec{r}_{\bar{\xi}\eta} = \vec{r}_{\xi\eta} \; / \; \frac{d\bar{\xi}}{d\xi} \; . \tag{22}$$

The interior stretching function devised by Vinokur [9] is as follows:

$$\bar{\xi} = \bar{\xi}_E + \frac{1}{\Delta y} \sinh^{-1} \left[\left(\frac{\xi}{\xi_E} - 1 \right) \sinh \left(\bar{\xi}_E \, \Delta y \right) \right] \; , \tag{23}$$

where

$$\bar{\xi}_E = \frac{1}{2\Delta y} \ln \frac{1 + \xi_E \left(e^{\Delta y} - 1 \right)}{1 - \xi_E \left(1 - e^{-\Delta y} \right)} \tag{24}$$

Then the derivative $d\bar{\xi}/d\xi$, obtained from Eq. (23), is

$$\frac{d\bar{\xi}}{d\xi} = \frac{\sinh \left(\bar{\xi}_E \, \Delta y \right)}{\xi_E \, \Delta y} \left[1 + \left(\frac{\xi}{\xi_E} - 1 \right)^2 \sinh^2 \left(\xi_E \, \bar{\Delta} y \right) \right] \; . \tag{25}$$

If the dimensionless slope at the inflection point ξ_E is S_E, i.e.

$$S_E = \frac{d\bar{\xi}}{d\xi} \left(\xi_E \right) \; ,$$

then S_E is found to be related to Δy by the following implicit equation:

$$\left(S_E \, \xi_E \, \Delta y \right)^{-2} = \frac{\cosh \Delta y - 1 + 1/\xi_E}{\sinh \Delta y} - 1. \tag{26}$$

Rather than specify S_E and solve Eq. (26) for Δy, we take the easier approach of specifying Δy and solving directly for S_E. By trial and

error a value of $\Delta y = 8$ has been found to produce adequately spaced radial curves with no folding near point E, as illustrated in Fig. 11.

Grid On Radial Surfaces

In the azimuthal plane, a radial curve may be defined in a discrete sense by the equations:

$$\left.\begin{aligned} y_j &= y(\hat{\eta}_j) \\ z_j &= z(\hat{\eta}_j) \end{aligned}\right\} \zeta = \text{constant}, \tag{27}$$

where the origin is taken at the polar axis through the tip, as shown in Fig. 11, and $\hat{\eta}$ is the running arc length of the radial curve. A radial surface is obtained, as already mentioned, by translating a radial curve from the initial value surface to the outflow plane. If flattened out, i.e., plotted as $\hat{\eta}$ versus x, it would appear as sketched in Fig. 12. On each radial surface a C-grid is generated in the x-$\hat{\eta}$ plane by conformal mapping and transfinite interpolation, the same procedure used for the surfaces of the fin grid.

Before a C-grid can be generated in the x-$\hat{\eta}$ plane, $\hat{\eta}$ of the tip must be determined as a function of x. Since the tip is assumed to be a half-body of revolution, for a given value of x its radius is constant. Thus a natural way of determining $\hat{\eta}_{tip}$ is to interpolate for $\hat{\eta}$ given r, the polar radius of each point on the radial curve. Lagrange cubic interpolation is used for this purpose.

Knowing $\hat{\eta}_{max}$ of a radial curve, the equivalent polar angle θ_{max} is computed from

$$\theta_{max} = \frac{\hat{\eta}_{max}}{r_T} , \tag{28}$$

from which the coordinate magnification F_M used in computing the C-grid is determined from

$$F_M = \frac{\pi}{\theta_{max}} \quad . \tag{29}$$

The above definition of F_M is dictated by the requirement of grid compatibility at the tip cylinder for the fin and tip regions. The magnified coordinates $(\bar{x},\bar{\theta})$ are given by:

$$\bar{x} = F_M(x - d_S) + \ln 2 \ , \tag{30}$$

$$\bar{\theta} = F_M\, \theta, \tag{31}$$

where d_S is the location of the singular point in the unwrapping transformation (see Eq. (10) of Ref. 7) and is just inside the leading edge of the airfoil. Thus when $\theta = \theta_{max}$, $\bar{\theta} = \pi$ which is a requirement of the unwrapping transformation.

Determination of the C-grid on a particular radial surface gives the $\hat{x}$-η coordinates of each nodal point, from which the y-z coordinates of the grid are determined by Lagrange cubic interpolation of the points defining the radial curve, Eq. (27).

3. RESULTS AND DISCUSSION

Finite span fin-afterbody grid generation using the present technique is performed by two computer codes totaling some 4200 FORTRAN statements. FINGRID generates the grid in the fin region (interior to the fin cylinder) while TIPGRID generates the grid in the tip region (between the tip and outer cylinders). Both codes are written in double precision arithmetic to minimize roundoff error from the many arithmetical operations required. Calculations are made in terms of

real variables only. At the present time there is no linkage between the two codes, i.e., the common grid on the tip cylinder is generated independently by each code. A User's Manual is incorporated in each FORTRAN listing by way of comment statements at the beginning.

As in Ref. 7, a NACA symmetric four-digit series airfoil was chosen to represent the fin section. The equation for this profile is, after slight modification of its original linear term to produce a zero thickness trailing edge:

$$z_F = -5\tau\ (0.2969\ \sqrt{x}\ - 0.1281x - 0.3516x^2 + 0.2843x^3 - 0.1015x^4) \qquad (32)$$

Because interpolation is used liberally on the airfoil in the grid generation process, an accurate definition of the thickness distribution, z_F vs. x, is required. For this purpose 101 points are used with clustering at the leading edge.

As a test problem to exhibit the characteristics of the method, an analytical afterbody was chosen, the same as in Ref. 7, given by the expression

$$r_B(t) = r_{B1}F(t) - d_{BOD}\tan\hat{\theta}_T G(t) \quad , \qquad (33)$$

where F and G are cubic blending functions given by Eq. (15), and

$$t = -\frac{x}{d_{BOD}} \quad .$$

The particular set of afterbody parameters, used in the test example, is as follows:

$$r_{B1} = 0.75 \quad , \quad d_{BOD} = 2.5 \quad , \quad \tan\hat{\theta}_T = 0.50 \quad .$$

This set produces a full afterbody profile with a tail half-angle of 26.6 degrees. Other parameters in the example are given in Table 1.

c_R	c_T	d_{BOD}	d_{IVLO}	d_{OB}	d_{TL}	r_{OC}	r_T	τ
1.3	0.8	2.5	0.3	1.0	0.5	4.0	1.2	0.2

Table 1. Parameters in Example 3-D Geometry.

A meridian plane view of the afterbody-fin geometry for the example is shown in Fig. 13 along with one intermediate tubular surface. This figure also contrasts the locus of point K along the fin using the circular arc method of Ref. 7 and the present method of requiring point K to lie along a specified fin generator line. The older method allows point K to migrate too close to the leading edge as the tip is apprcached which results in a squeezing of grid lines intersecting the fin from the initial value surface.

Figures 14 - 16 present different perspective views of the body, intermediate and tip grid surfaces of the example. Also shown is the outline of the fin. In this example grid lines are clustered at the fin leading edge, point K, the fin trailing edge and body tail point. Figure 17 is a view of the grid on the fin symmetry plane, fin surface and body surface. The intent of this figure is to show the smoothness of the grid in the stacking direction.

Perspective views in the tip region are presented in Figs. 18-20 showing the grid on the tip cylinder, fin plane of symmetry and outflow

plane. Nine curved radial surfaces were used in the stacking direction (azimuthally). Figure 21 shows a view similar to the previous three except the grid has been truncated in the downstream direction at the surface through point K.

The grid on the outflow plane and surface through point K is seen to have a kink at the curve passing through the corner formed by the intersection of the outer cylinder and 45 degree symmetry plane. This feature is, unfortunately, an integral part of the grid topology. Figure 18, a more nearly head on view, clearly shows the nature of the stacked grid. The skewness of the grid is seen to increase as the kink is approached and can be attributed to the use of the same clustering parameters on each C-grid. By varying certain of these parameters azimuthally the smoothness in the stacking direction should improve.

The procedure in its present form suffers from one other shortcoming, namely, that due to the simplified tip geometry (a half body of revolution) surface derivatives across the fin-tip juncture are not smooth. This defect can be corrected by refining the definition of the tip geometry and modifying the C-grid accordingly in the tip region.

REFERENCES

1. L. E. Eriksson, "Generation of Boundary-Conforming Grids Around Wing-Body Configurations Using Transfinite Interpolation," AIAA Jour., 20:1313-1320 (1982).

2. R. E. Smith, Jr., E. L. Everton and R. A. Kudlinski, "Algebraic Grid Generation for Wing-Fuselage Bodies," AIAA Paper 84-0002, presented at AIAA 22nd Aerospace Sci. Meeting, Reno, NV (9-12 Jan. 1984).

3. P. R. Eiseman, "Three-Dimensional Coordinates About Wings," AIAA Paper 79-1461, presented at AIAA Fluid Dynamics Conf., Williamsburg, VA (23-25 July 1979).

4. D. A. Caughey and A. Jameson, "Numerical Calculation of Transonic Potential Flow About Wing-Body Combinations," AIAA Jour., 17:175-181 (1979).

5. A. Shmilovich and D. A. Caughey, "Grid Generation for Wing-Tail-Fuselage Configurations," in Advances in Grid Generation, ASME FED - Vol. 5, pp. 189-197, presented at Appl. Mech., Bioengin. and Fluids Engin. Conf., Houston, TX (20-22 June 1983).

6. N. D. Halsey, "Conformal Mapping as an Aid in Grid Generation for Complex Three-Dimensional Configurations," AIAA Paper 86-0497, presented at AIAA 24th Aerospace Sci. Meeting, Reno, NV (6-9 Jan. 1986).

7. G. H. Hoffman, "A Combination Conformal-Transfinite Mapping Method for Grids About Fin-Afterbody Combinations," Applied Math. & Computation, to appear (1986).

8. M. Vinokur and K. Lombard, "Algebraic Grid Generation with Corner Singularities," in Advances in Grid Generation, ASME FED - Vol. 5, pp. 99-106, presented at Appl. Mech., Bioengin. and Fluids Engin. Conf., Houston, TX (20-22 June 1983).

9. M. Vinokur, "On One-Dimensional Stretching Functions for Finite-Difference Calculations," Jour. Comp. Phys., 50:215-269 (1983).

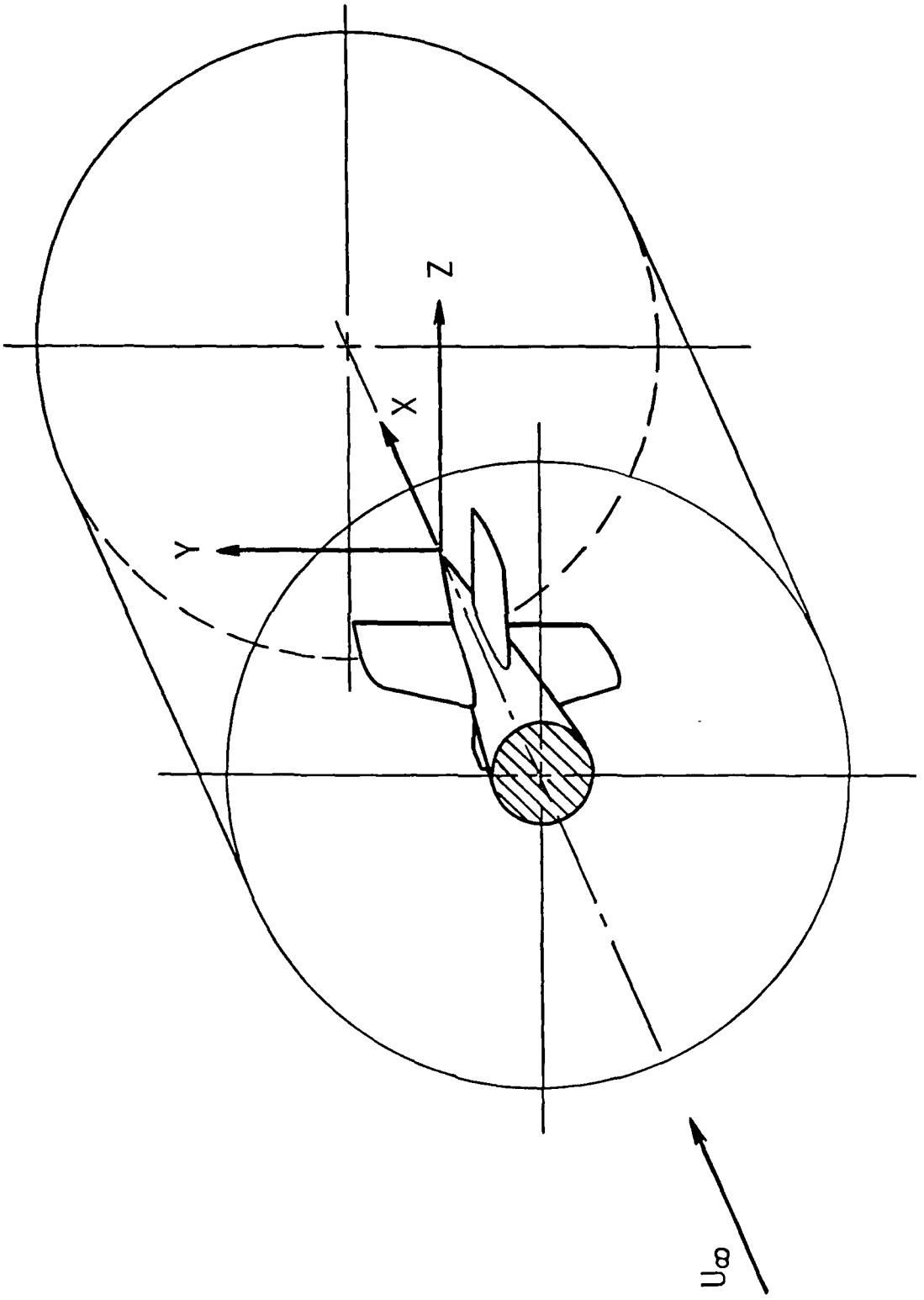

Figure 1. Schematic of Geometry and Computational Domain.

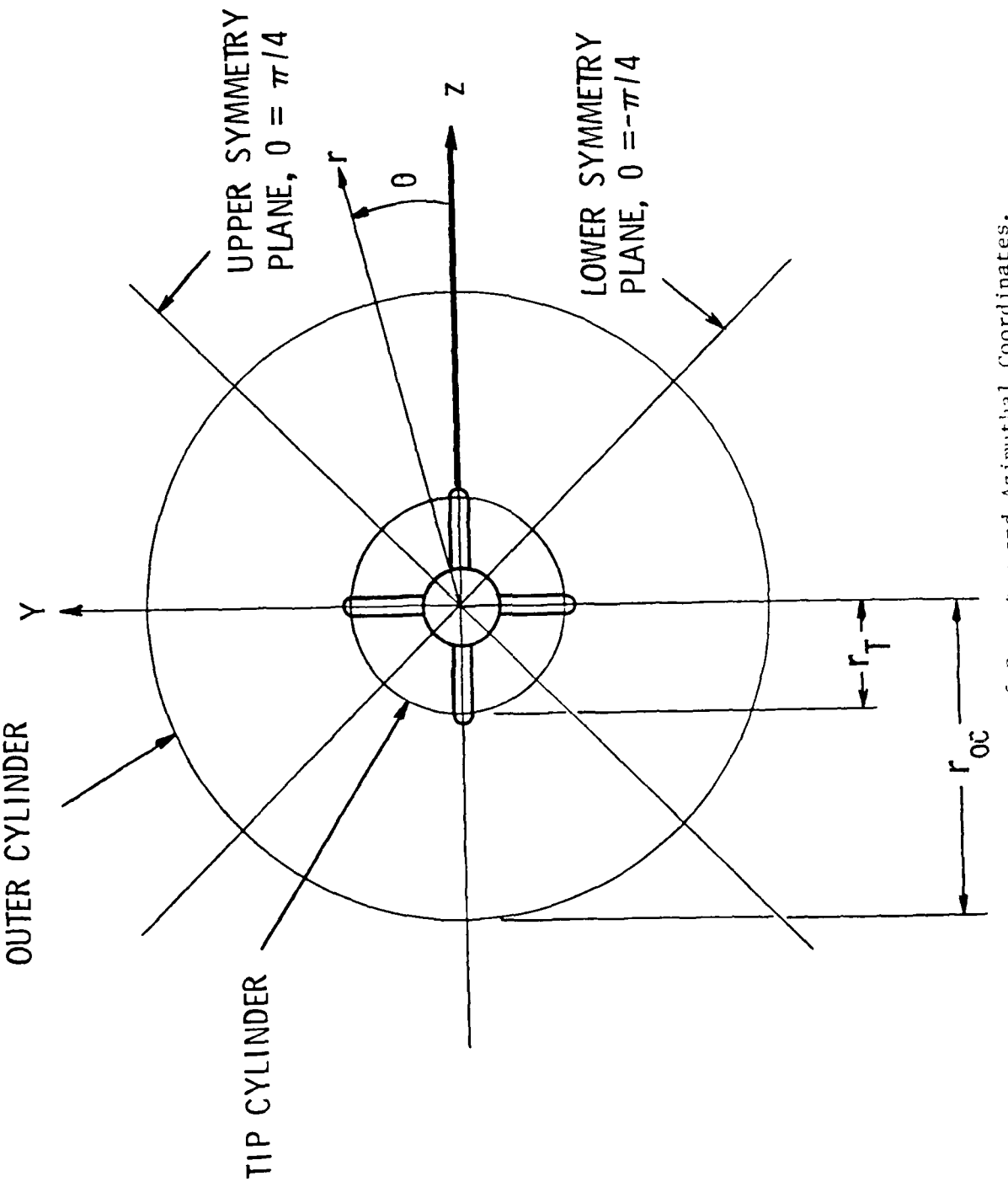

Figure 2. Planes of Symmetry and Azimuthal Coordinates.

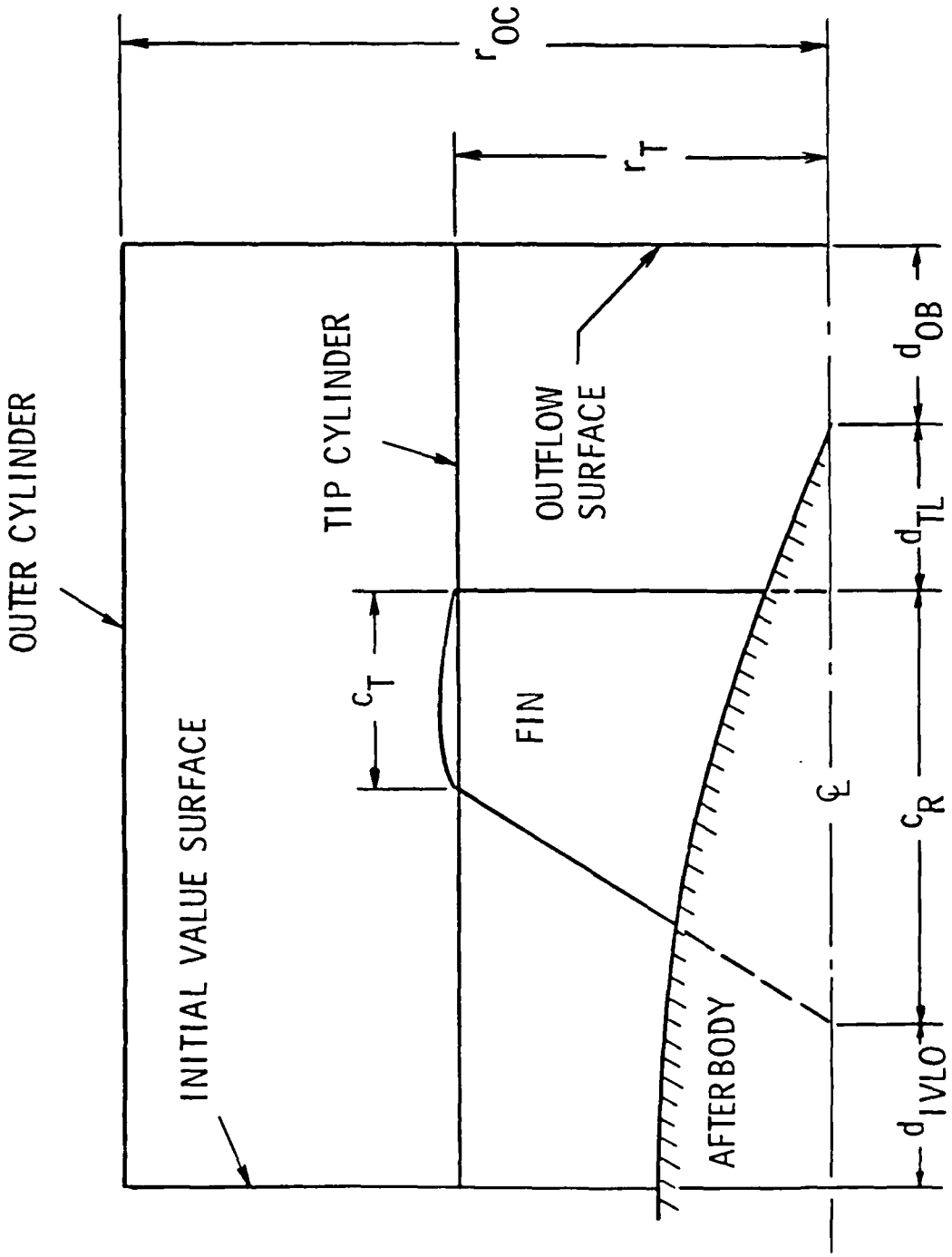

Figure 3. Meridian Plane Schematic of Geometry.

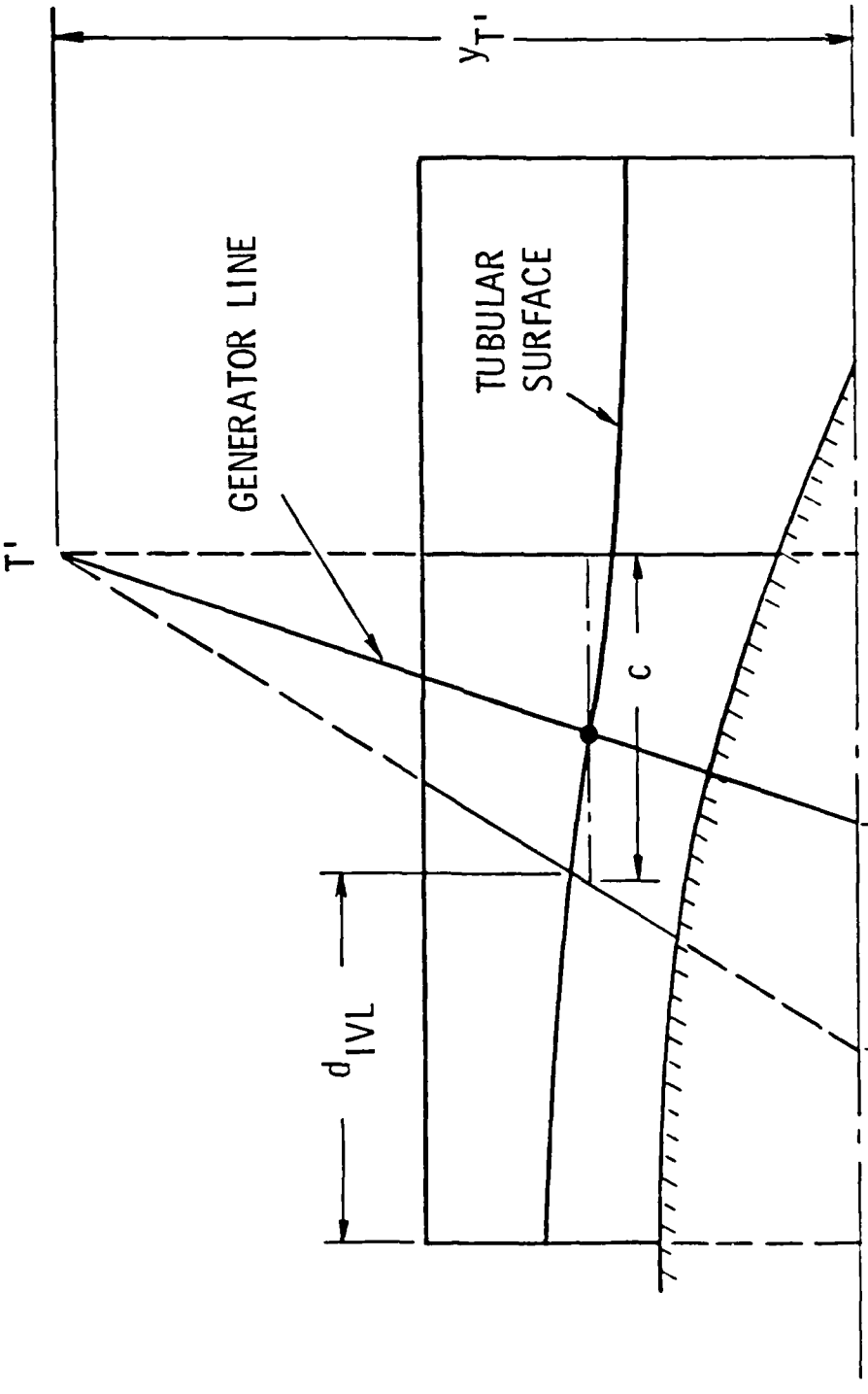

Figure 4. Fin-Tubular Surface Intersection, Meridian Plane.

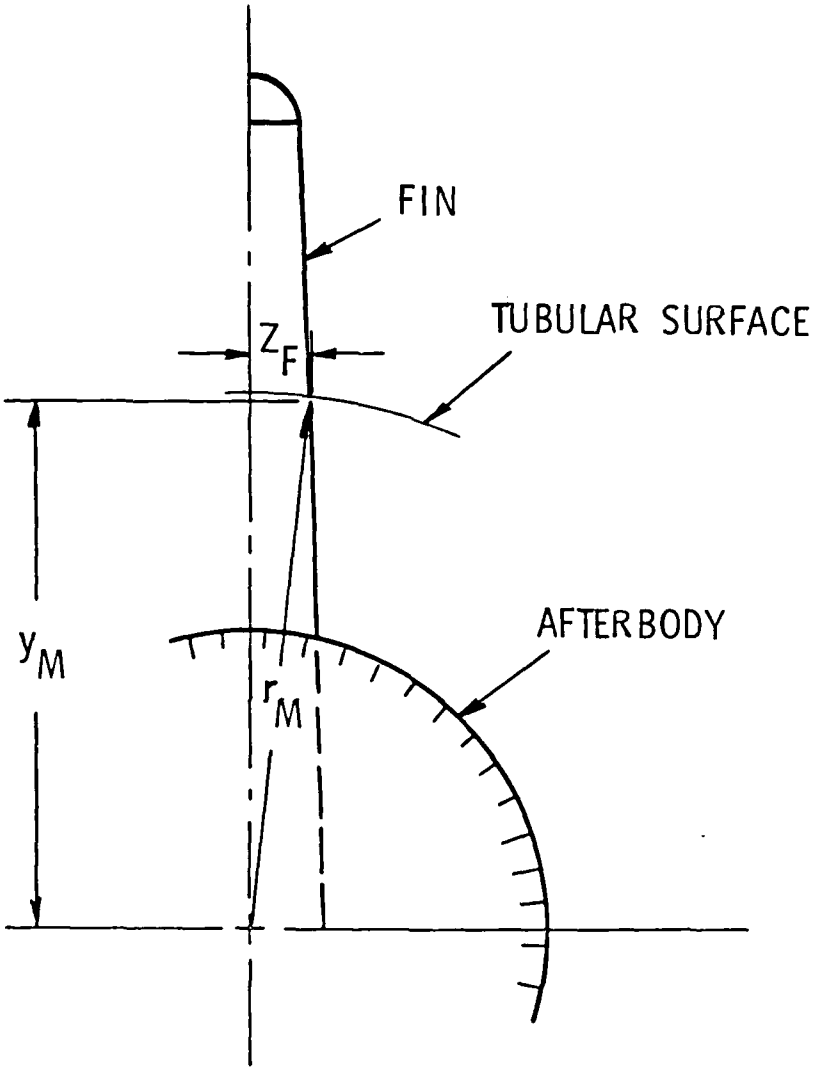

Figure 5. Fin-Tubular Surface Intersection, Azimuthal Plane.

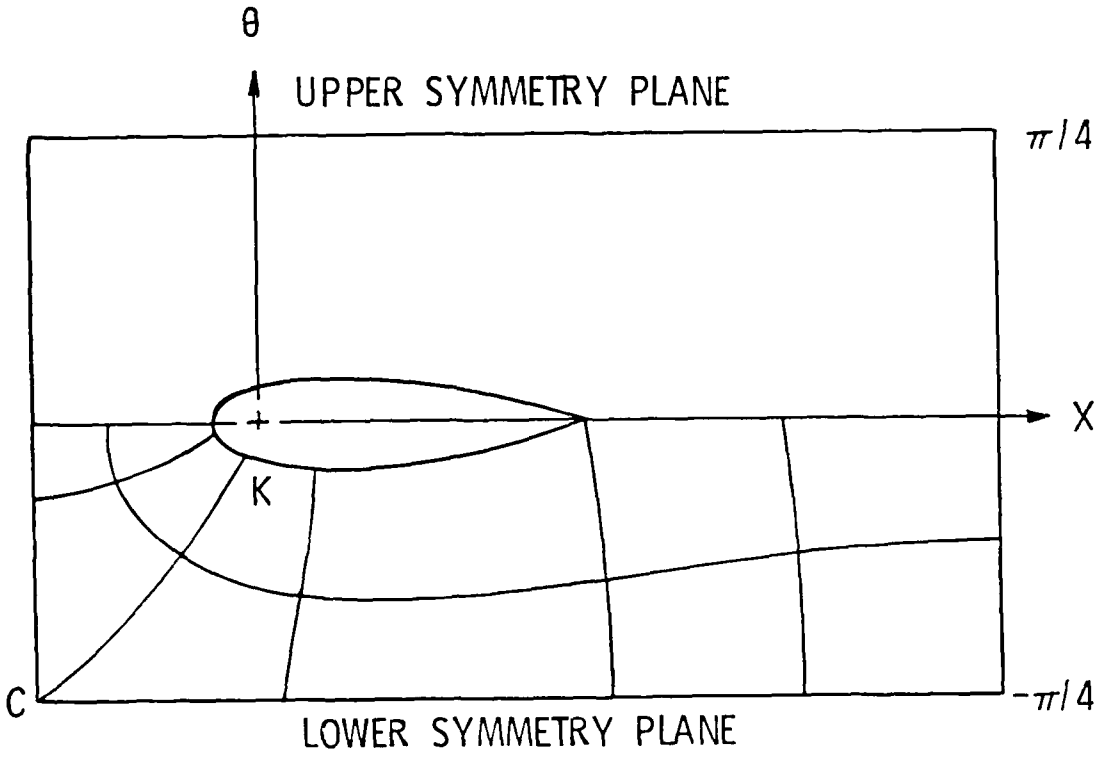

Figure 6. Computational Domain on Unwrapped Tubular Surface.

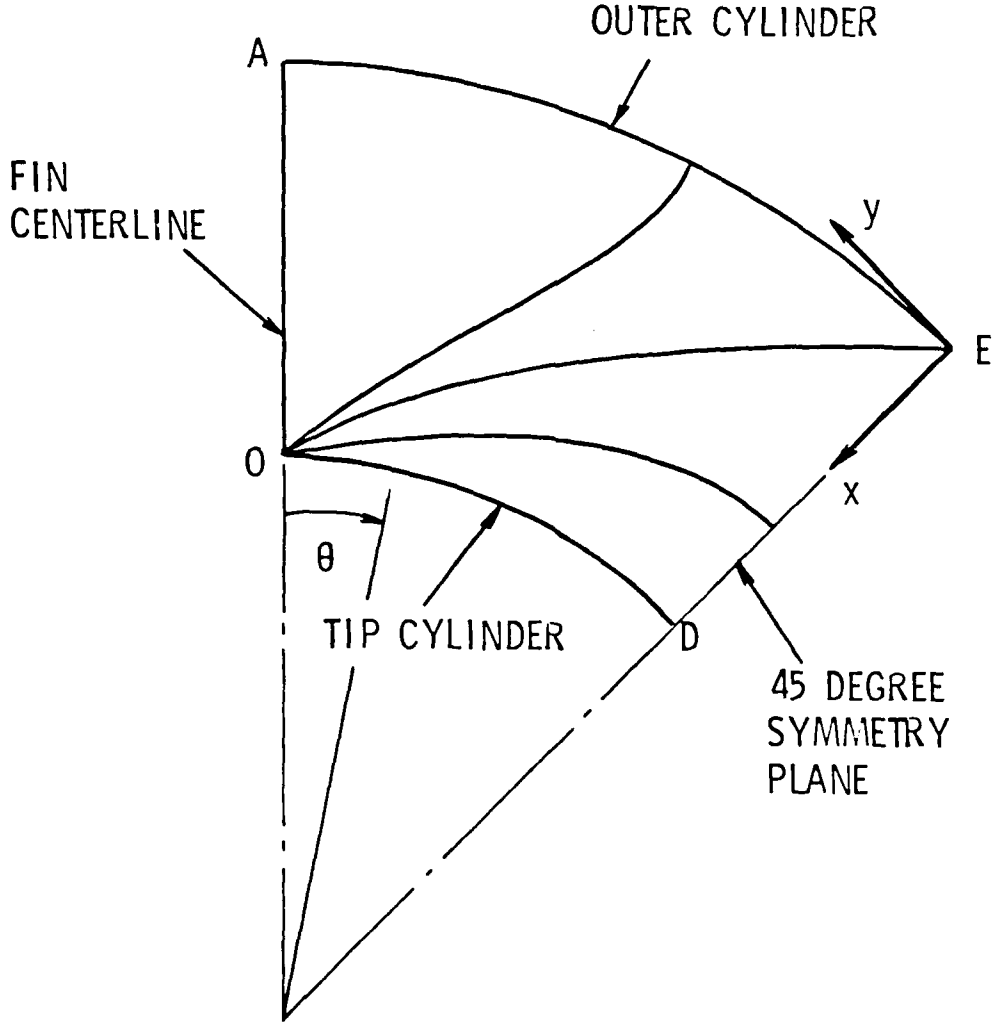

Figure 7. Topology of Polar Grid Curves in Azimuthal Plane.

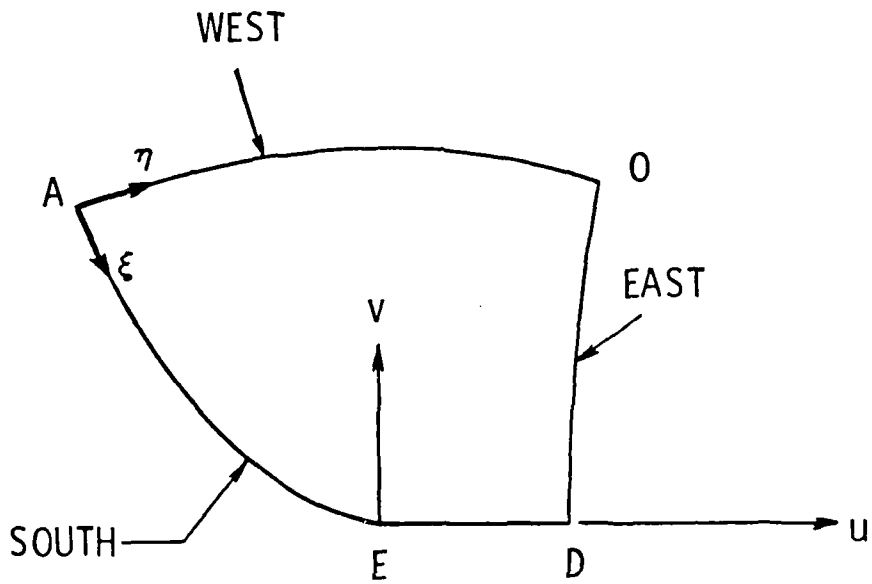

Figure 8. Image of Tip Grid Boundary in Hinge Plane.

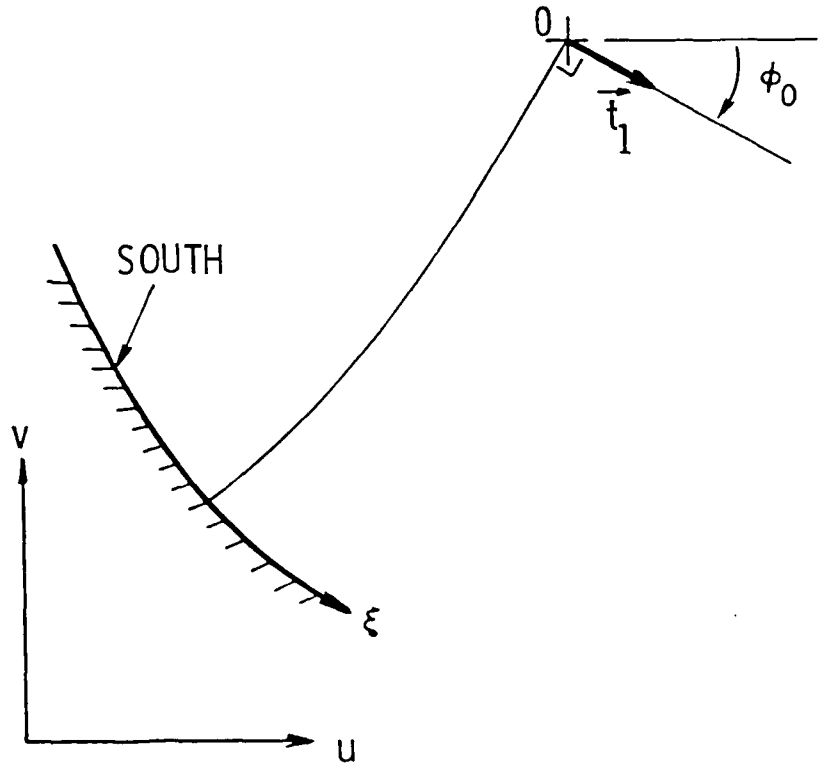

Figure 9. Turning Angle at Point 0 of ξ = Constant Line.

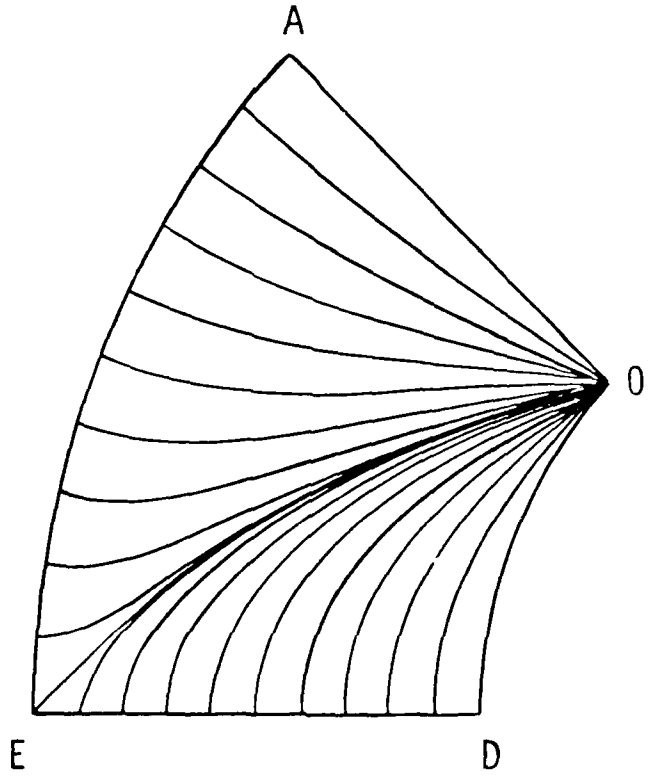

Figure 10. Radial Curves in Tip Region Showing Folding Near O-E.

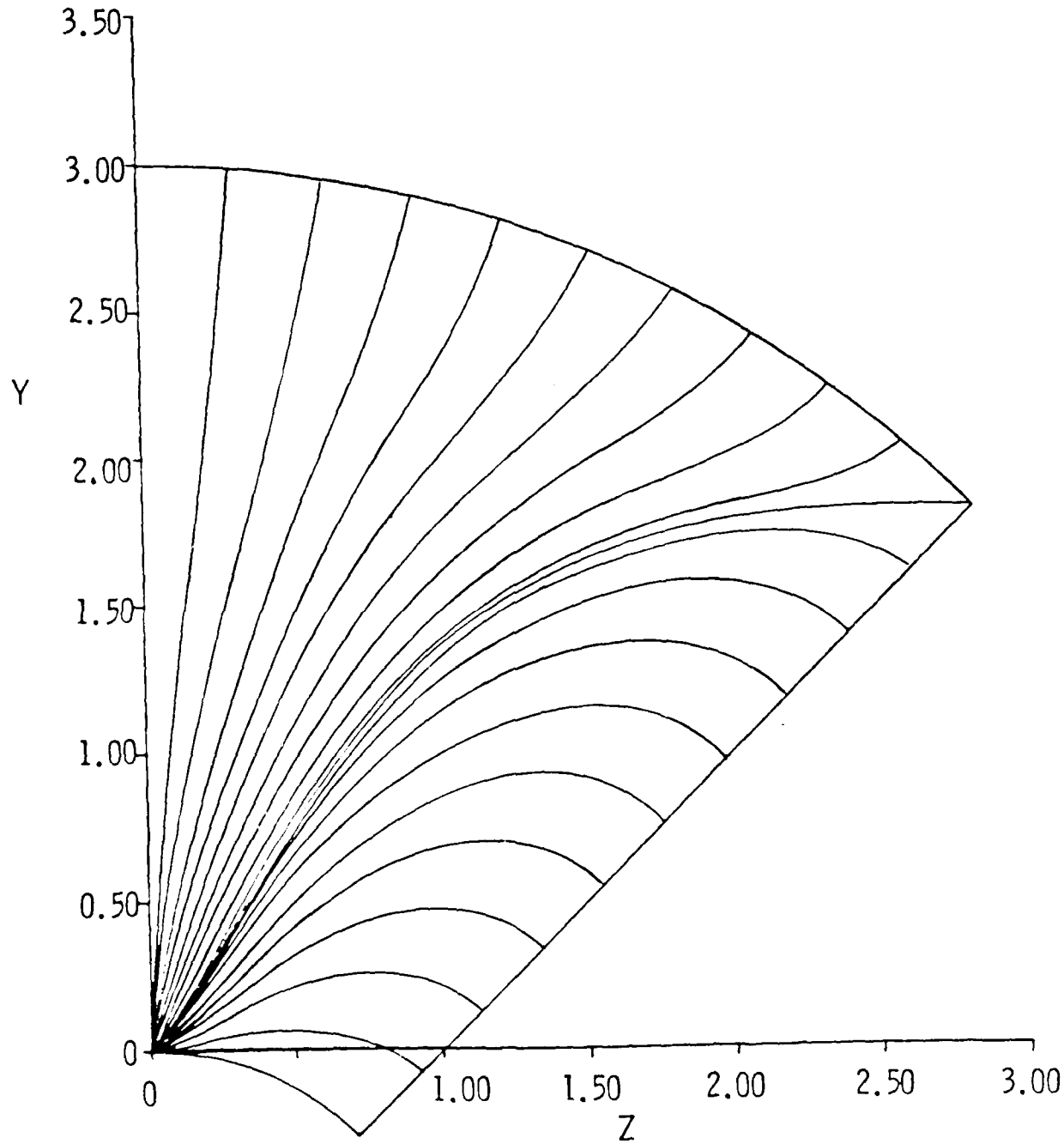

Figure 11. Radial Curves in Tip Region Without Folding.

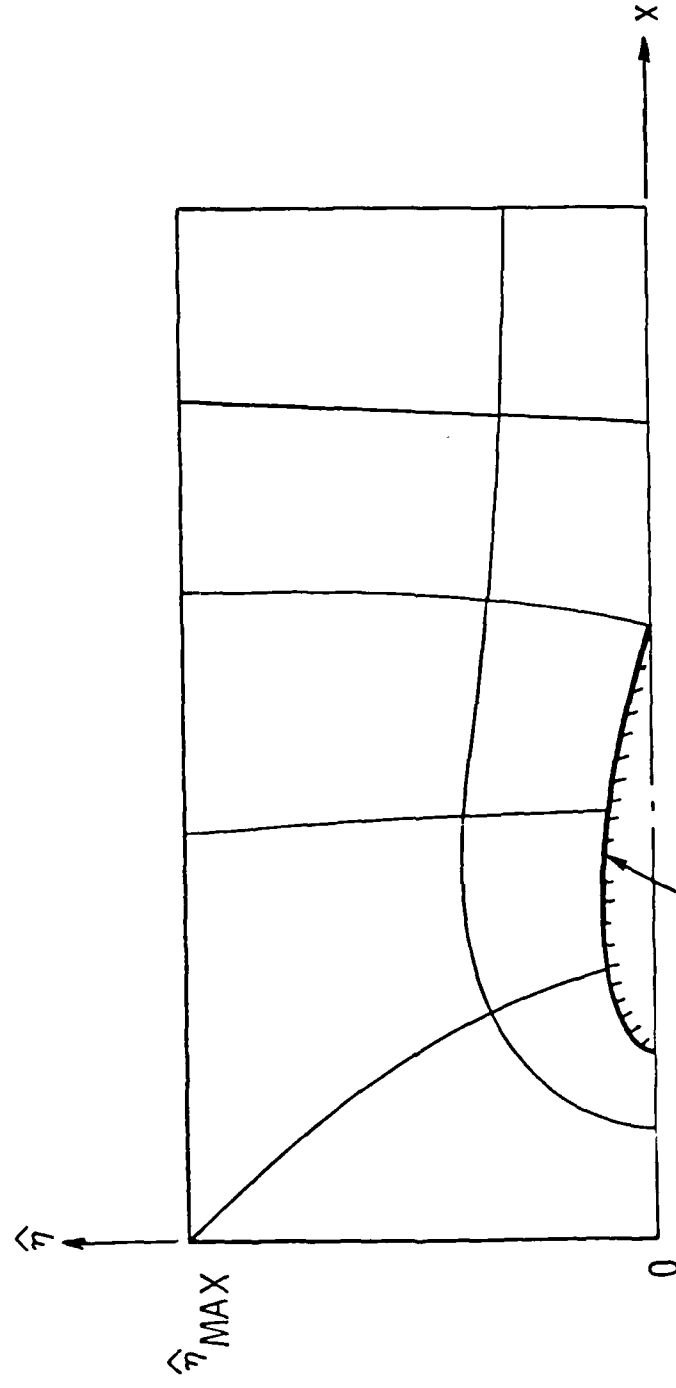

Figure 12. Flattened Radial Surface.

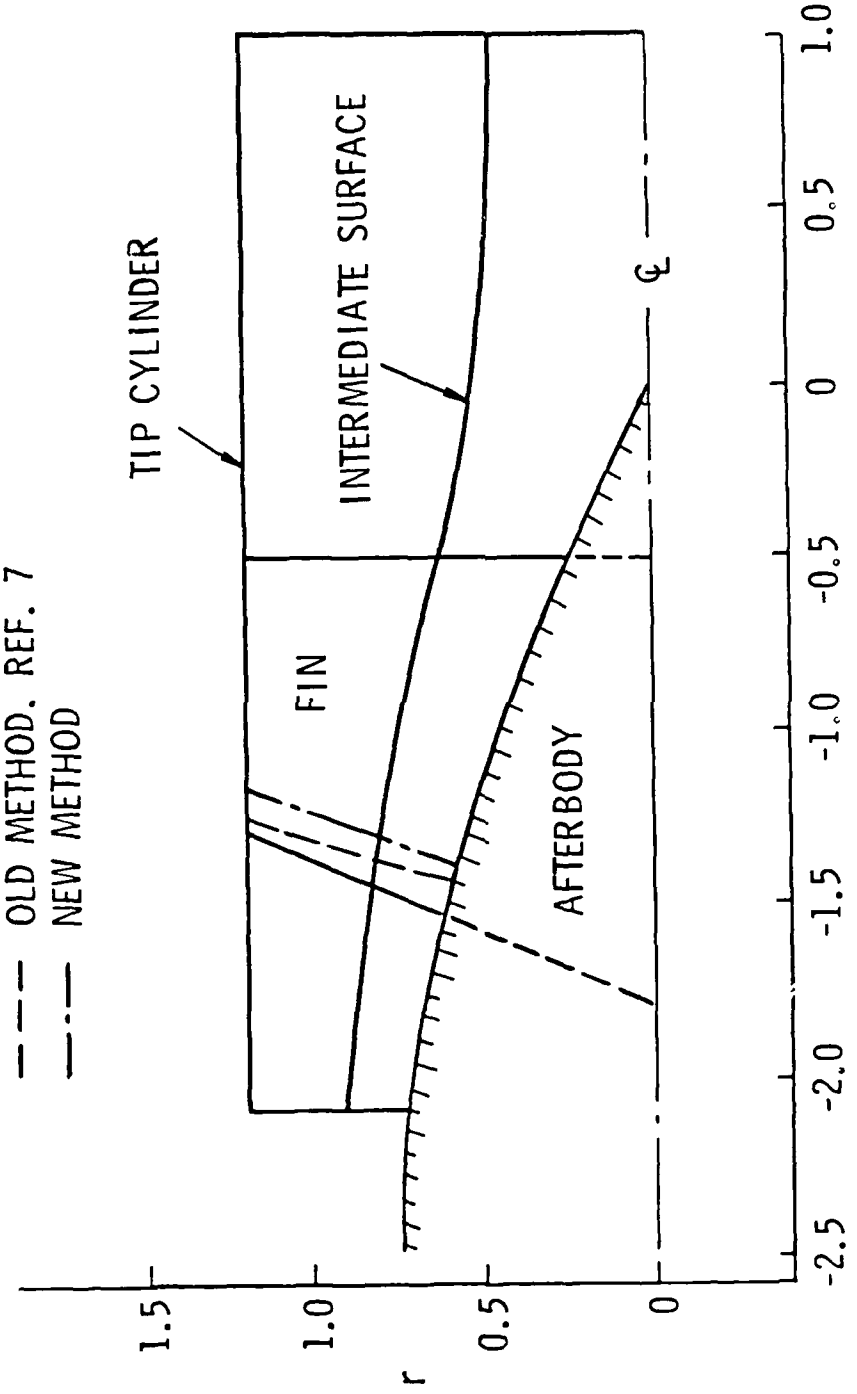

Figure 13. Meridian Plane View of Test Problem Geometry.

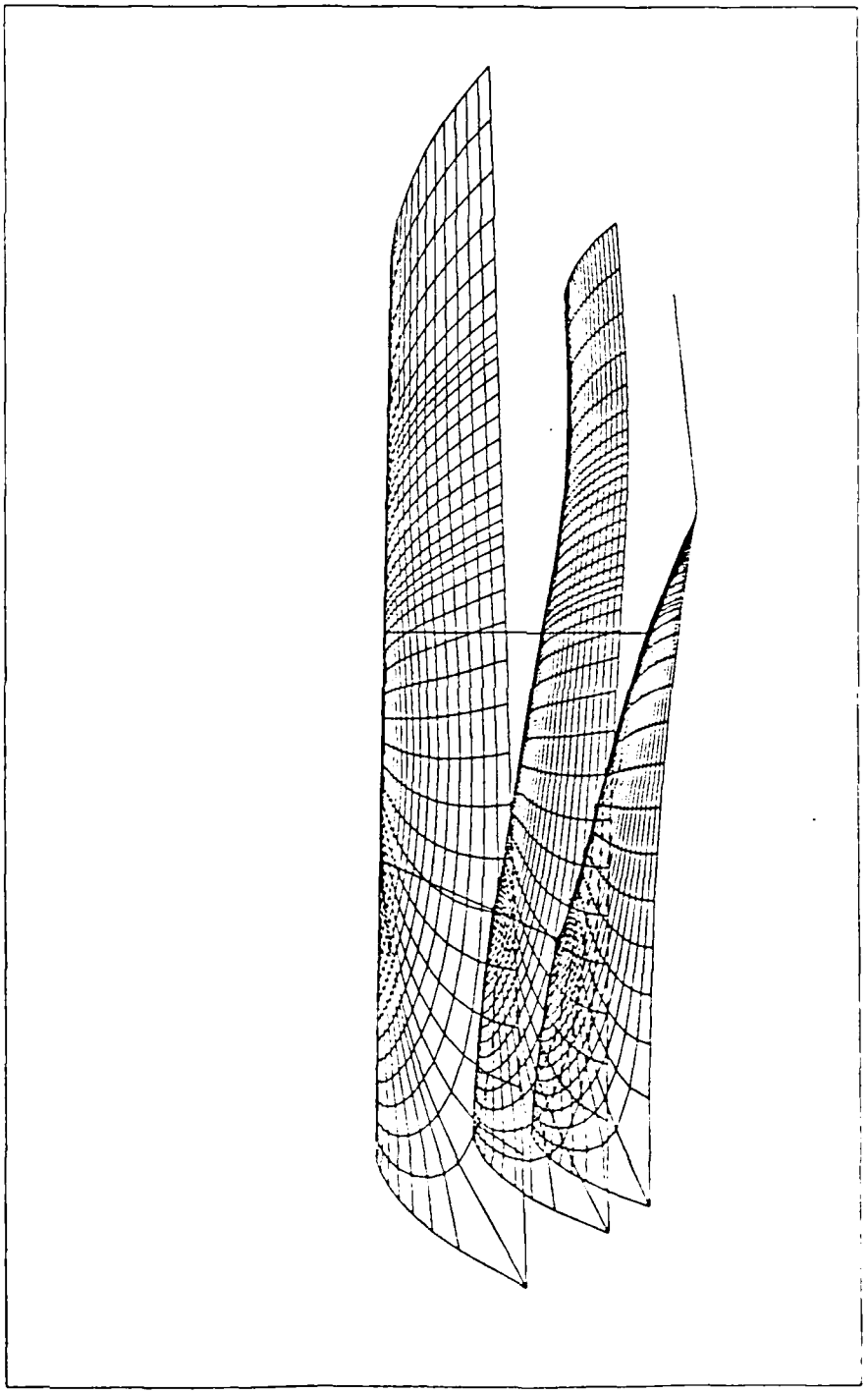

Figure 14. Side View of Fin Grid.

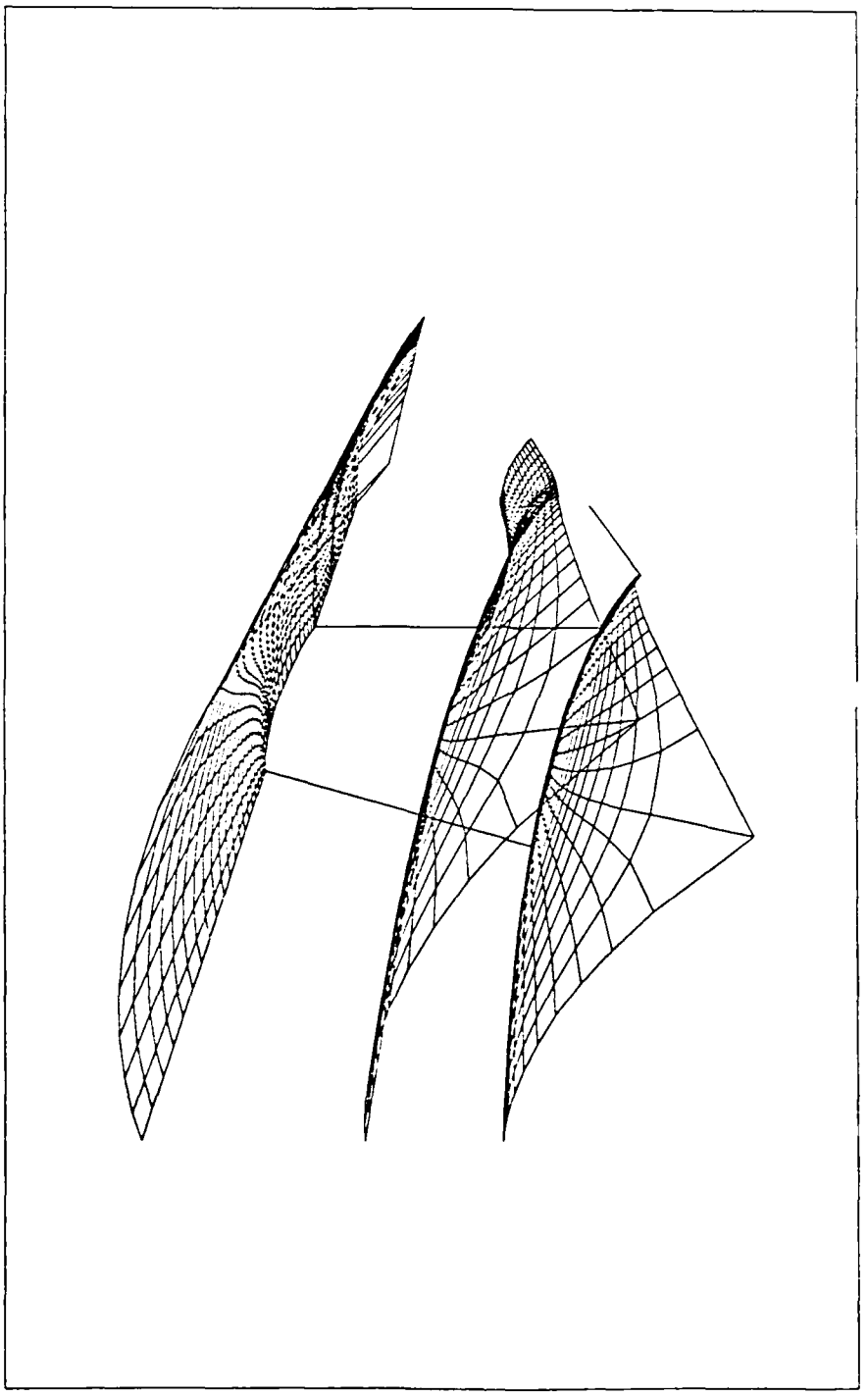

Figure 15. Nearly Head on View of Fin Grid.

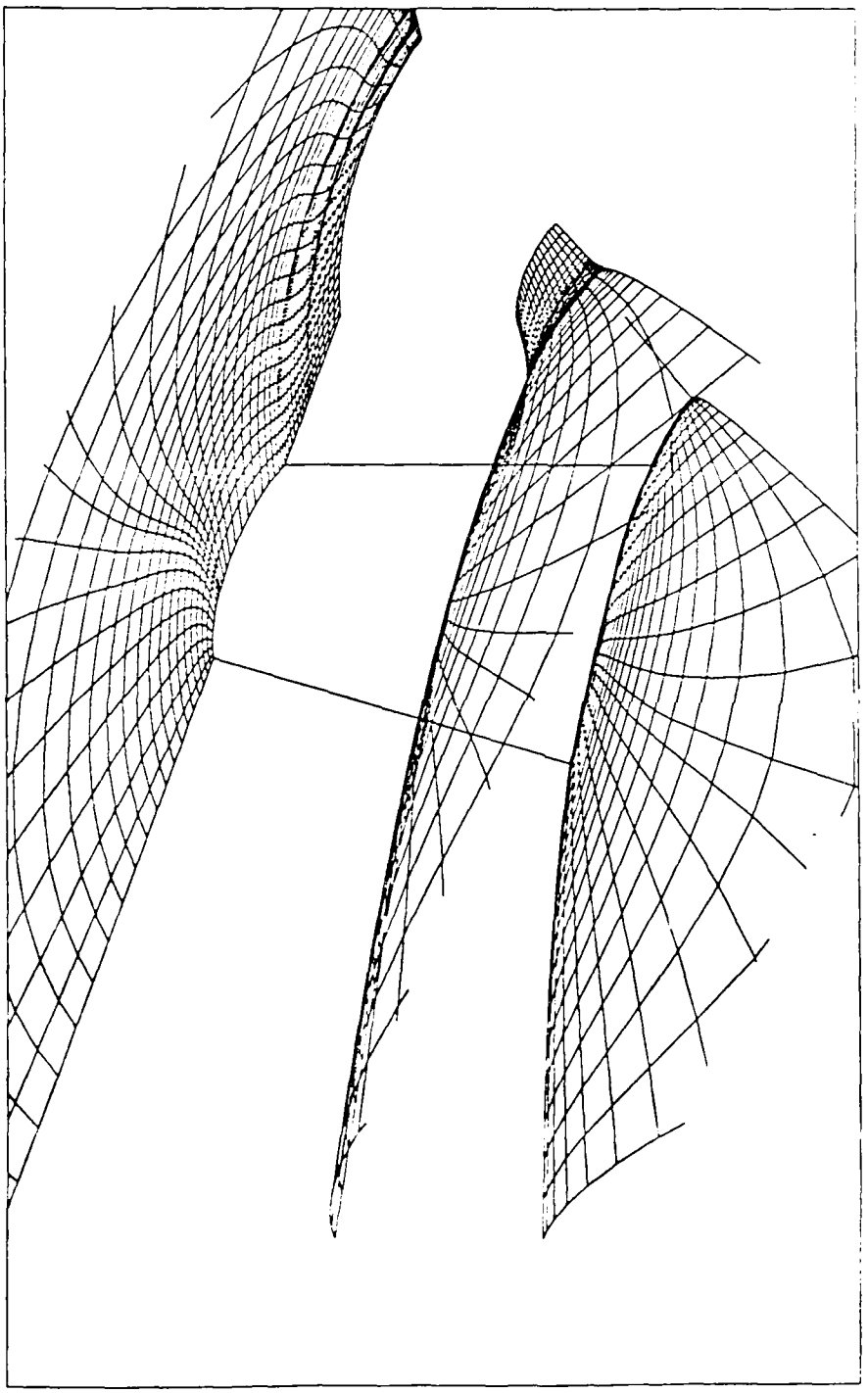

Figure 16. Close Up View of Fin Grid.

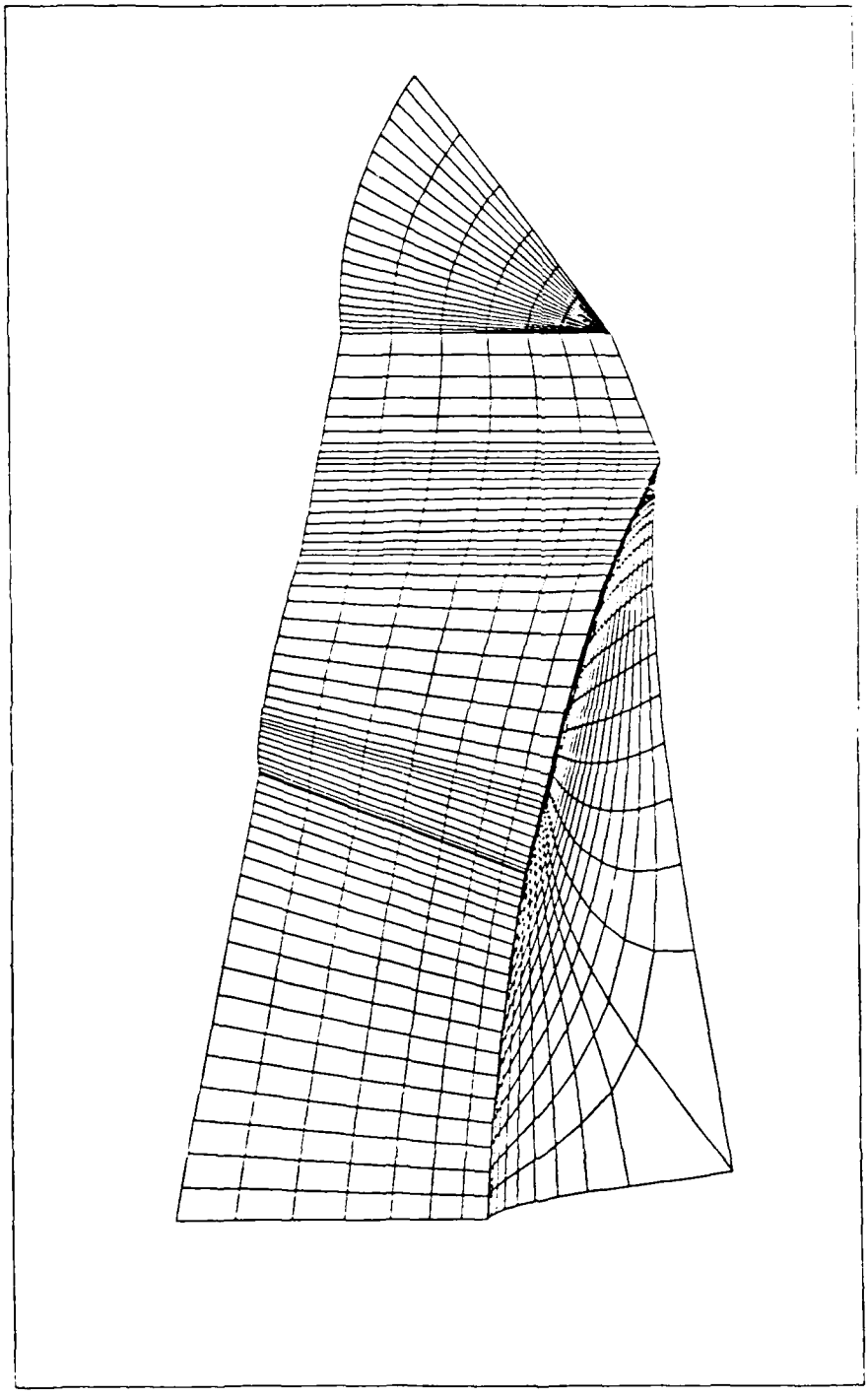

Figure 17. Grid on Body, Fin and Symmetry Plane.

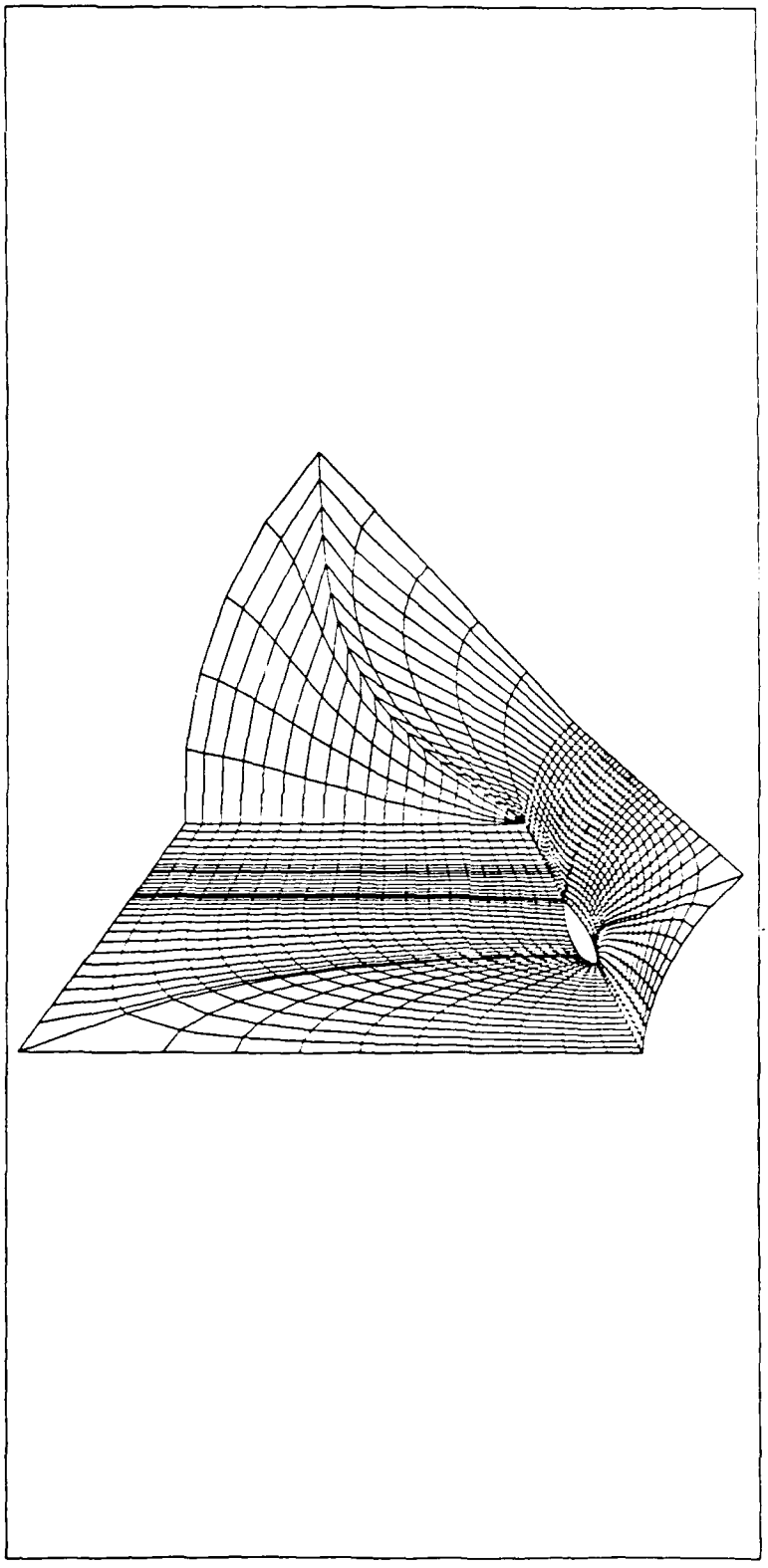

Figure 18. Nearly Head On View of Tip Grid.

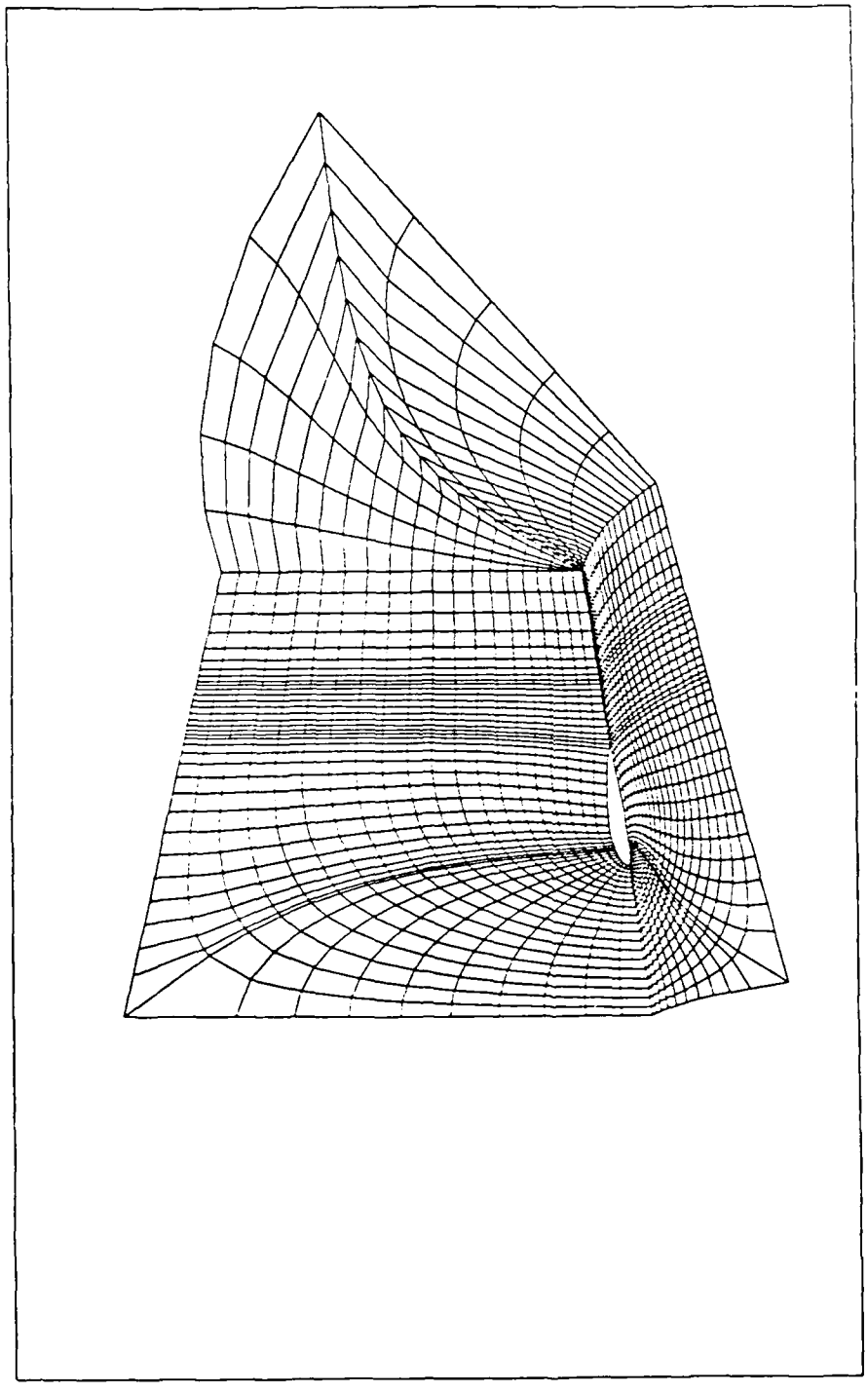

Figure 19. Side View of Tip Grid.

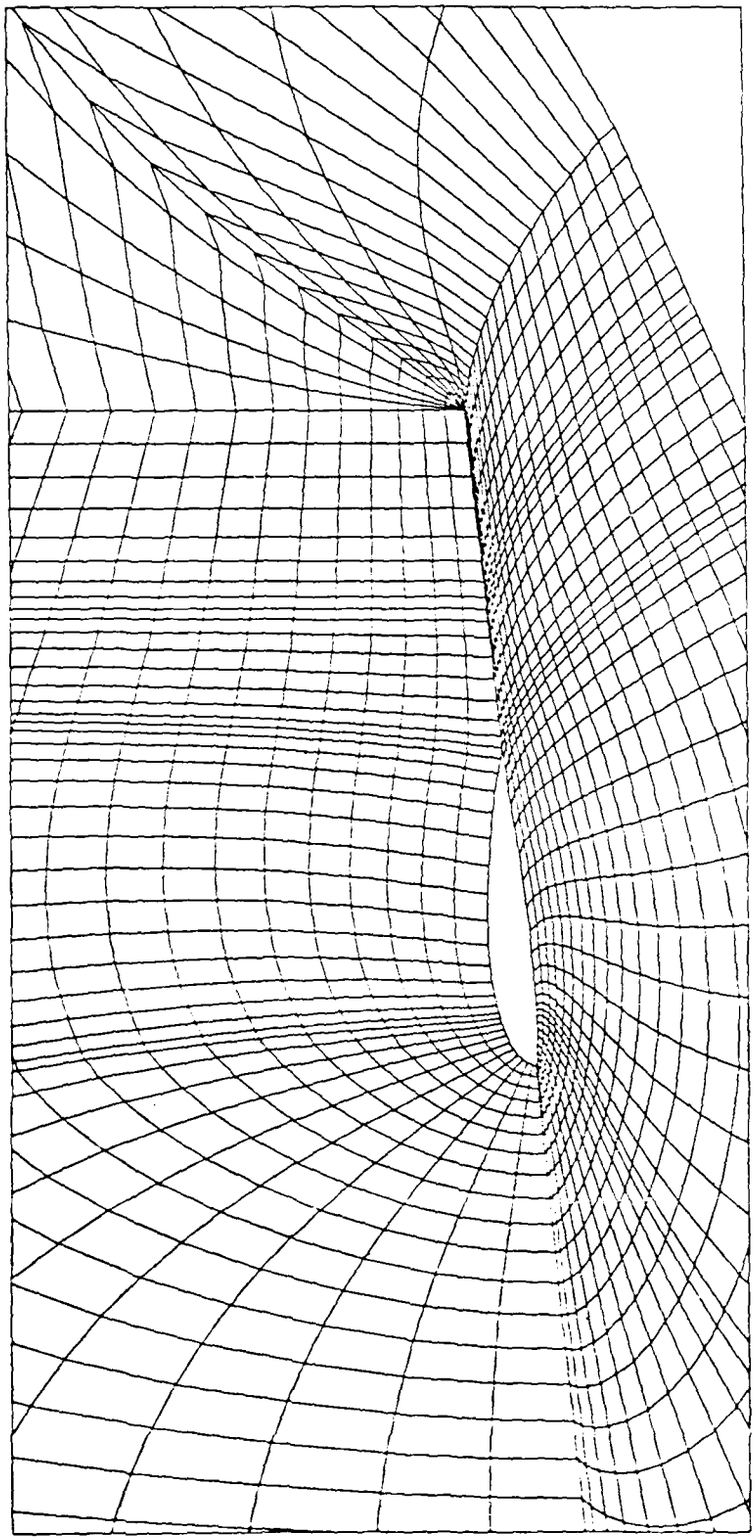

Figure 20. Close Up of Tip Grid.

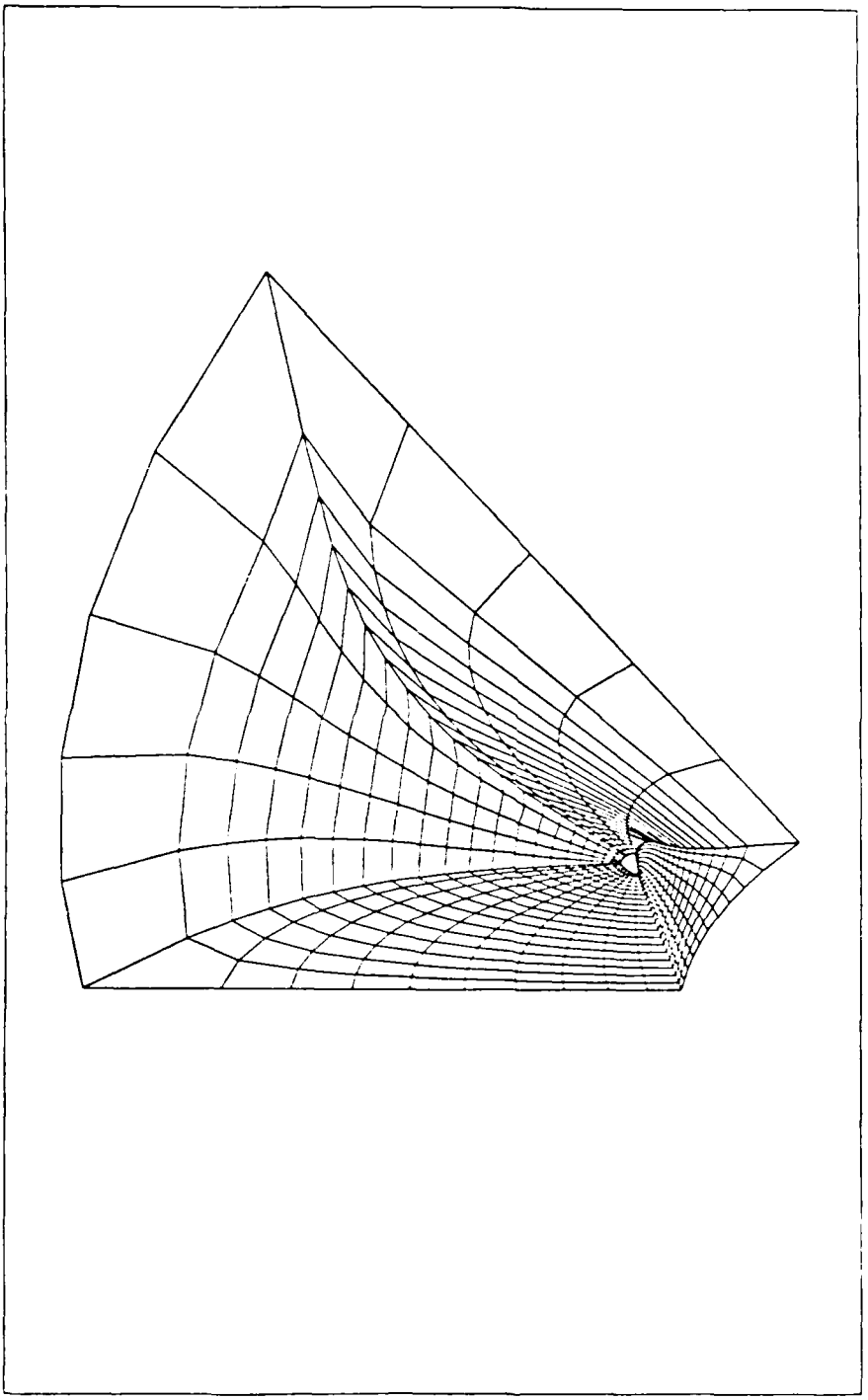

Figure 21. Tip Grid Showing Surface Through Point K.

END

1-87

DTIC